INTERNATIONAL JOURNAL FOR NUMERICAL METHODS IN FLUIDS, VOL. 16, 629–654 (1993)

FLUX DIFFERENCE SPLITTING FOR OPEN-CHANNEL FLOWS

P. GLAISTER

Department of Mathematics, P.O. Box 220, University of Reading, Whiteknights, Reading RG6 2AX, U.K.

SUMMARY

A finite difference scheme based on flux difference splitting is presented for the solution of the one-dimensional shallow-water equations in open channels, together with an extension to two-dimensional flows. A linearized problem, analogous to that of Riemann for gas dynamics, is defined and a scheme, based on numerical characteristic decomposition, is presented for obtaining approximate solutions to the linearized problem. The method of upwind differencing is used for the resulting scalar problems, together with a flux limiter for obtaining a second-order scheme which avoids non-physical, spurious oscillations. The scheme is applied to a one-dimensional dam-break problem, and to a problem of flow in a river whose geometry induces a region of supercritical flow. The scheme is also applied to a two-dimensional dam-break problem. The numerical results are compared with the exact solution, or other numerical results, where available.

KEY WORDS Shallow-water equations Subcritical and supercritical flows Open channels

1. INTRODUCTION

The flow of water in a channel with (local) rectangular cross-section and smoothly varying bottom surface is governed by the one-dimensional shallow-water equations for open channels. The assumption of hydrostatic pressure distribution is used in deriving these equations.[1] Since analytical solutions of these equations are not generally available, they are solved numerically. Computational models of river flow based on the so-called St. Venant equations of open-channel flow are a well-established tool in engineering practice. Such models can provide quantitative information on discharge, velocity and level for a variety of purposes including flood defence design, navigation, flood forecasting, flood plain zoning, dam-break analysis and irrigation scheme control.

Several explicit and implicit finite difference methods have been used to solve the shallow-water equations.[2–4] One feature of this set of hyperbolic equations is the formation of bores, i.e. discontinuous solutions, which can be difficult to represent accurately even if a shock-capturing method is used. The most popular scheme in the hydraulic engineering community is the implicit method of Preissman.[5] However, this scheme does not perform well in the presence of discontinuities. Finite element methods have also been applied to these equations (see, for example Reference 6).

In the field of unsteady gas dynamics governed by the Euler equations, where shocks are frequently present, some authors have designed finite difference schemes that have good shock-capturing properties (see, for example, Reference 7). These schemes solve linearized Riemann

0271–2091/93/070629–26$18.00

Received February 1992
Revised November 1992

problems using upwind differencing and flux limiters to obtain shocks that are spread over two or three mesh points. An alternative approach to flux difference splitting was proposed by Vila[8] for the equations of isentropic gas dynamics and has been applied with success to the shallow-water equations.[9] The scheme of Godunov[10] solves Riemann problems exactly using an iterative procedure. Vila simplifies this iteration using approximate Riemann invariants, and achieves second-order accuracy by considering generalized Riemann problems, i.e. ones where the data are assumed to be piecewise linear discontinuous. However, this scheme does not apply to open-channel flows. In contrast, the scheme in Reference 7 applies upwind differencing to a specially constructed set of scalar problems. Second-order accuracy is then achieved using classical second-order scalar schemes, limited to avoid non-physical oscillations in the solution.

In this paper a new scheme is presented for the open-channel flow equations that incorporates the ideas mentioned earlier for the Euler equations, and an extension to the two-dimensional equations is also given. Although the derivation of this scheme is detailed, its implementation is straightforward. The resulting algorithm is efficient and produces satisfactory results for a problem of geometry-induced supercritical flow in a river, together with a one- and a two-dimensional dam-break problem.

2. GOVERNING EQUATIONS

The St. Venant equations governing the rough turbulent flow of water in an open channel can be written as

$$\mathbf{w}_t + \mathbf{f}_x = \mathbf{b}, \tag{1}$$

where

$$\mathbf{w} = (A, Q)^{\mathrm{T}}, \tag{2a}$$

$$\mathbf{f}(\mathbf{w}) = \left(Q, \frac{Q^2}{A}\right)^{\mathrm{T}} \tag{2b}$$

and

$$\mathbf{b}(\mathbf{w}) = \left[0, -gA\left(\frac{\partial h}{\partial x} + \frac{Q|Q|}{K^2}\right)\right]. \tag{2c}$$

The quantities $A = A(x, t)$ and $Q = Q(x, t) = Au(x, t)$ represent the cross-sectional area and mass flow, respectively, at a general position x measured along the channel, and at time t, where u is the fluid velocity. The gravitational constant is represented by g. We consider the case where the channel is locally rectangular, so that

$$A = B(x)d(x, t),$$

where B is the breadth and d the depth. The height is then $h = h(x, t) = d(x, t) + z(x)$, where z is the height of the river bed. Also $K = A/M$ (hydraulic radius)$^{2/3}$, where Manning's constant M is taken as 0·03, and the hydraulic radius $= A/$(wetted perimeter) $= A/(2A/B + B)$. Equations (1)–(2c) can then be written, after some manipulation, as

$$\mathbf{w}_t + \mathbf{f}_x + D\mathbf{h}_x = \mathbf{c}, \tag{3}$$

where

$$\mathbf{w} = (A, Au)^{\mathrm{T}}, \tag{4a}$$

$$(\mathbf{f}(\mathbf{w}) = (Au, Au^2)^{\mathrm{T}}, \tag{4b}$$

as above,

$$\mathbf{h}(\mathbf{w})=\left(0,\frac{A^2}{2}\right)^{\mathrm{T}}, \tag{4c}$$

$$D=\begin{pmatrix}0 & 0\\ 0 & g/B\end{pmatrix} \tag{4d}$$

and

$$\mathbf{c}(\mathbf{w})=\left[0, g\frac{A^2}{B^2}B'(x)-gAz'(x)-0{\cdot}0009gAu|u|\left(\frac{A}{2A/B+B}\right)^{-4/3}\right]^{\mathrm{T}}. \tag{4e}$$

Equation (3) has been written so that the right-hand side does not contain any derivatives of the flow variables A and $Q=Au$.

3. LINEARIZED RIEMANN PROBLEM

If the approximate solution of equations (3)–(4e) is sought using a finite difference method then the solution is known at a set of discrete mesh points $(x, t)=(x_j, t_n)$ at any time $t=t_n$. Following Godunov,[10] the approximate solution $\mathbf{w}_j^n$ to $\mathbf{w}$ at (x_j, t_n) can be considered as a set of piecewise constants $\mathbf{w}=\mathbf{w}_j^n$ for $x\in(x_j-\Delta x/2, x_j+\Delta x/2)$ at time t_n, where $\Delta x=x_j-x_{j-1}$ is a constant mesh spacing. A Riemann problem is now present at each interface $x_{j-1/2}=\frac{1}{2}(x_{j-1}+x_j)$ separating adjacent states $\mathbf{w}_{j-1}^n$, $\mathbf{w}_j^n$. If the shallow-water equations are linearized by considering the Jacobian matrices of the flux functions $\mathbf{f}$ and $\mathbf{h}$ to be constant in each interval (x_{j-1}, x_j), the resulting equations can be solved approximately using explicit time stepping, and this is described in Section 4. The time step Δt is restricted so that the solutions of adjacent Riemann problems do not interact. The scalar problems that result from this analysis can be solved by upwind differencing; however, an approximate Jacobian matrix needs to be constructed in each interval so that shock capturing is automatic.

4. APPROXIMATE RIEMANN SOLVER

4.1. Linearization

Consider the interval $[x_{j-1}, x_j]\equiv[x_{\mathrm{L}}, x_{\mathrm{R}}]$ and denote by $\mathbf{w}_{\mathrm{L}}, \mathbf{w}_{\mathrm{R}}$ the approximations to $\mathbf{w}$ at $x_{\mathrm{L}}, x_{\mathrm{R}}$, respectively. We now rewrite equation (3) as

$$\mathbf{w}_t+\frac{\partial\mathbf{f}}{\partial\mathbf{w}}\mathbf{w}_x+D\frac{\partial\mathbf{h}}{\partial\mathbf{w}}\mathbf{w}_x=\mathbf{c}(\mathbf{w}), \tag{5}$$

and solve approximately the associated linearized Riemann problem

$$\mathbf{w}_t+(\tilde{F}+\tilde{D}\tilde{H})\mathbf{w}_x=\mathbf{c}(\mathbf{w}), \tag{6}$$

with data $\mathbf{w}_{\mathrm{L}}, \mathbf{w}_{\mathrm{R}}$ either side of the point $x_{j-1/2}$, where the matrices $\tilde{F}(\mathbf{w}_{\mathrm{L}}, \mathbf{w}_{\mathrm{R}})$, $\tilde{D}(\mathbf{w}_{\mathrm{L}}, \mathbf{w}_{\mathrm{R}})$ and $\tilde{H}(\mathbf{w}_{\mathrm{L}}, \mathbf{w}_{\mathrm{R}})$ are constant. We then use the approximate form of equation (6):

$$\frac{\mathbf{w}_P^{n+1}-\mathbf{w}_P^n}{\Delta t}+(\tilde{F}+\tilde{D}\tilde{H})\frac{(\mathbf{w}_{\mathrm{R}}^n-\mathbf{w}_{\mathrm{L}}^n)}{\Delta x}=\tilde{\mathbf{c}}(\mathbf{w}^n), \tag{7}$$

where $\tilde{\mathbf{c}}$ is an approximation to $\mathbf{c}$, and P may be L or R. The matrix $\tilde{D}$ is assumed to have the form

$$\tilde{D}=\begin{bmatrix}0 & 0\\ 0 & g/\tilde{B}\end{bmatrix}, \tag{8}$$

where $\tilde{B}$ is an average of $B(x_L)$ and $B(x_R)$. The matrices $\tilde{F}$ and $\tilde{H}$ are approximations to the Jacobian matrices

$$F=\frac{\partial \mathbf{f}}{\partial \mathbf{w}}(\mathbf{w}) \quad \text{and} \quad H=\frac{\partial \mathbf{h}}{\partial \mathbf{w}}(\mathbf{w}),$$

respectively, and are constructed so that

$$\tilde{F}\,\Delta\mathbf{w}=\Delta\mathbf{f} \tag{9a}$$

and

$$\tilde{H}\,\Delta\mathbf{w}=\Delta\mathbf{h} \tag{9b}$$

for all arbitrary jumps $\Delta\mathbf{w}$, where $\Delta(\cdot)=(\cdot)_R-(\cdot)_L$. This ensures that the scheme is conservative and shock capturing.

4.2. Construction

The solution of this problem is straightforward to determine and is given by

$$\tilde{F}=\begin{bmatrix} 0 & 1 \\ -\tilde{u}^2 & 2\tilde{u} \end{bmatrix} \tag{10a}$$

and

$$\tilde{H}=\begin{bmatrix} 0 & 0 \\ \tilde{A} & 0 \end{bmatrix}, \tag{10b}$$

where $\tilde{u}$ denotes the square root mean of left and right states of u, namely,

$$\tilde{u}=\frac{\sqrt{(A_L)}u_L+\sqrt{(A_R)}u_R}{\sqrt{(A_R)}+\sqrt{(A_L)}}, \tag{11}$$

and $\tilde{A}$ denotes the arithmetic mean of left and right states, namely,

$$\tilde{A}=\tfrac{1}{2}(A_L+A_R) \tag{12}$$

(see the Appendix for a detailed derivation of equations (11) and (12)). Since no specific average $\tilde{B}$ results, we take

$$\tilde{B}=\tfrac{1}{2}(B_L+B_R)=\tfrac{1}{2}[B(x_L)+B(x_R)] \tag{13}$$

for computational efficiency.

4.3. Approximation for $\tilde{\mathbf{c}}$

Following the averages determined above, a natural approximation for $\tilde{\mathbf{c}}$ can be obtained from equations (4e) and (11)–(13) as

$$\tilde{\mathbf{c}}=\left[0,\, g\frac{\tilde{A}^2}{\tilde{B}^2}\frac{\Delta B}{\Delta x}-g\tilde{A}\frac{\Delta z}{\Delta x}-0{\cdot}0009g\tilde{A}\tilde{u}|\tilde{u}|\left(\frac{\tilde{A}}{2\tilde{A}/\tilde{B}+\tilde{B}}\right)^{-4/3}\right]^{\mathrm{T}}. \tag{14}$$

4.4. Projection

To complete the Riemann solver it is necessary to project $\mathbf{w}_R^n-\mathbf{w}_L^n$ and $\tilde{\mathbf{c}}$ (given above) in equation (7) onto the eigenvectors of $\tilde{F}+\tilde{D}\tilde{H}$.

Firstly, the eigenvalues of $\tilde{F}+\tilde{D}\tilde{H}$ are

$$\tilde{\lambda}_{1,2}=\tilde{u}\pm\sqrt{\frac{g\tilde{A}}{\tilde{B}}}, \tag{15a, b}$$

with associated eigenvectors

$$\tilde{\mathbf{e}}_{1,2}=\left(1,\ \tilde{u}\pm\sqrt{\frac{g\tilde{A}}{\tilde{B}}}\right)^{\mathrm{T}}. \tag{16a, b}$$

(Note that the matrix $\partial\mathbf{f}/\partial\mathbf{w}+D(\partial\mathbf{h}/\partial\mathbf{w})=F+DH$ has eigenvalues and eigenvectors given by equations (15a)–(16b) in the limit $\mathbf{w}_{\mathrm{L}}, \mathbf{w}_{\mathrm{R}}\rightarrow\mathbf{w}$.) Projecting

$$\Delta\mathbf{w}=\mathbf{w}_{\mathrm{R}}^{n}-\mathbf{w}_{\mathrm{L}}^{n}=\sum_{i=1}^{2}\tilde{\alpha}_i\tilde{\mathbf{e}}_i, \tag{17}$$

we find that

$$\tilde{\alpha}_{1,2}=\frac{1}{2}\left(\Delta A\pm\frac{\hat{A}}{\tilde{A}}\Delta u\right), \tag{18a, b}$$

where

$$\hat{A}=\sqrt{(A_{\mathrm{L}}A_{\mathrm{R}})}. \tag{19}$$

Thus, in equation (7)

$$(\tilde{F}+\tilde{D}\tilde{H})\Delta\mathbf{w}=\sum_{i=1}^{2}\tilde{\lambda}_i\tilde{\alpha}_i\tilde{\mathbf{e}}_i \tag{20}$$

since $\tilde{F}+\tilde{D}\tilde{H}$ has eigenvalues $\tilde{\lambda}_i$ with eigenvectors $\tilde{\mathbf{e}}_i$. Similarly, if we project

$$\tilde{\mathbf{c}}=-\frac{1}{\Delta x}\sum_{i=1}^{2}\tilde{\beta}_i\tilde{\mathbf{e}}_i, \tag{21}$$

then

$$\beta_1=-\beta_2=\frac{g\tilde{A}\,\Delta z-g\dfrac{\tilde{A}^2}{\tilde{B}^2}\Delta B+0{\cdot}0009g\,\Delta x\tilde{A}\tilde{u}|\tilde{u}|\left[\dfrac{\tilde{A}}{2\tilde{A}/\tilde{B}+\tilde{B}}\right]^{-4/3}}{2\sqrt{g\tilde{A}/\tilde{B}}}, \tag{22a, b}$$

so that equation (7) may be written as

$$\frac{\mathbf{w}_{\mathrm{P}}^{n+1}-\mathbf{w}_{\mathrm{P}}^{n}}{\Delta t}+\frac{\sum_{i=1}^{2}\tilde{\lambda}_i\tilde{\alpha}_i\tilde{\mathbf{e}}_i}{\Delta x}=-\frac{1}{\Delta x}\sum_{i=1}^{2}\tilde{\beta}_i\tilde{\mathbf{e}}_i \tag{23}$$

or

$$\frac{\mathbf{w}_{\mathrm{P}}^{n+1}-\mathbf{w}_{\mathrm{P}}^{n}}{\Delta t}+\frac{\sum_{i=1}^{2}\tilde{\lambda}_i\gamma_i\tilde{\mathbf{e}}_i}{\Delta x}=\mathbf{0}, \tag{24}$$

where $\tilde{\gamma}_i=\tilde{\alpha}_i+\tilde{\beta}_i/\tilde{\lambda}_i$, Δx and Δt represent the mesh spacings in the x and t directions, respectively, and the point P may be L or R. Upwind differencing now applied to equation (24) gives the following first-order algorithm for the solution of equations (3)–(4e):

$$\begin{aligned}&\text{add } -\frac{\Delta t}{\Delta x}\tilde{\lambda}_i\tilde{\gamma}_i\tilde{\mathbf{e}}_i \text{ to } \mathbf{w}_{\mathrm{R}} \text{ when } \tilde{\lambda}_i>0\\ \text{or}\\ &\text{add } -\frac{\Delta t}{\Delta x}\tilde{\lambda}_i\tilde{\gamma}_i\tilde{\mathbf{e}}_i \text{ to } \mathbf{w}_{\mathrm{L}} \text{ when } \tilde{\lambda}_i<0.\end{aligned} \tag{25}$$

Thus, we note the direction of flow of information given by the approximate eigenvalues $\tilde{\lambda}_i$ and use this information to update the solution consistent with the theory of characteristics of equation (3). In addition, second-order transfers of these first-order increments can be made to achieve higher accuracy, providing they are limited to maintain monotonicity.[11] The use of these 'flux-limiters' improves accuracy without introducing non-physical spurious oscillations, especially at bores. To allow depression waves to be treated correctly, the first-order increment can be considered as two separate increments being sent to either end of the cell.[12]

5. EXTENSION TO TWO DIMENSIONS

The two-dimensional St. Venant equations governing open-channel flows can be written in conservation form as

$$\hat{\mathbf{w}}_t + \hat{\mathbf{F}}_x + \hat{\mathbf{G}}_z = \hat{\mathbf{f}} + \hat{\mathbf{g}}, \tag{26}$$

where

$$\hat{\mathbf{w}} = (\phi, \phi u, \phi w)^{\mathrm{T}}, \tag{27a}$$

$$\hat{\mathbf{F}}(\mathbf{w}) = \left(\phi u, \phi u^2 + \frac{\phi^2}{2}, \phi uw\right)^{\mathrm{T}}, \tag{27b}$$

$$\hat{\mathbf{G}}(\mathbf{w}) = \left(\phi w, \phi uw, \phi w^2 + \frac{\phi^2}{2}\right), \tag{27c}$$

$$\hat{\mathbf{f}}(\mathbf{w}) = [0, g\phi(h_x - s_x), 0]^{\mathrm{T}}, \tag{28a}$$

$$\hat{\mathbf{g}}(\mathbf{w}) = [0, 0, g\phi(h_z - s_z)]^{\mathrm{T}} \tag{28b}$$

and

$$\phi = g(\eta + h). \tag{29}$$

The quantities $\phi = \phi(x, z, t)$ and $u = u(x, z, t)$ and $w = w(x, z, t)$ represent g multiplied by the total height above the bottom of the channel and the components of the fluid velocity in the x- and z-direction, respectively, at a general position x, z and at time t. The gravitational constant is represented by g and the undisturbed depth of the water is given by $h(x, z)$. The elevation $\eta = \eta(x, z, t)$ above the plane $y = 0$ is measured in the vertical y-direction. The quantities s_x, s_z are the slopes of the energy grade lines in the x- and z-direction, respectively, and are determined from the steady-state friction formulae (in SI units):

$$s_x = \frac{n^2 u\sqrt{(u^2 + w^2)}}{(\phi/g)^{4/3}}, \tag{30a}$$

$$s_z = \frac{n^2 w\sqrt{(u^2 + w^2)}}{(\phi/g)^{4/3}}, \tag{30b}$$

where n represents Manning's roughness coefficient. Alternatively, the following form could be used:

$$s_x = \frac{gu\sqrt{(u^2 + w^2)}}{\phi C^2}, \tag{31a}$$

$$s_z = \frac{gw\sqrt{(u^2 + w^2)}}{\phi C^2}, \tag{31b}$$

where C is Chézy's flow friction coefficient.

We propose solving equation (26) using similar ideas to those given in Section 4, in particular, the technique of operator splitting, i.e. solve successively

$$\hat{\mathbf{w}}_t + \hat{\mathbf{F}}_x = \hat{\mathbf{f}} \tag{32a}$$

and

$$\hat{\mathbf{w}}_t + \hat{\mathbf{G}}_z = \hat{\mathbf{g}} \tag{32b}$$

along the x- and z-co-ordinate lines, respectively, noting that the vectors $\hat{\mathbf{f}}$ and $\hat{\mathbf{g}}$ are associated with the x- and z-direction, respectively. We give the scheme for the solution of equation (32a) and the scheme for the solution of equation (32b) will then follow by symmetry.

Following the approach outlined in Section 4, a first-order, explicit numerical scheme for equation (32a) along an x-co-ordinate line $z = z_0$ can be written as

$$\hat{\mathbf{w}}_k^{m+1} = \hat{\mathbf{w}}_k^m - \frac{\Delta t}{\Delta x} \sum_{i=1}^{3} \tilde{\lambda}_i \tilde{\gamma}_i \tilde{\mathbf{e}}_i, \tag{33}$$

where Δt, Δx represent mesh spacings in the t- and x-direction, respectively, $\hat{\mathbf{w}}_j^m$ represents the numerical approximation to the solution $\hat{\mathbf{w}}(x_j, z_0, m\Delta t)$, after m time steps, and at a point x_j on this co-ordinate line. The value of k depends on the sign of each $\tilde{\lambda}_i$ (see below) as the technique of upwinding is employed, i.e. k could be j or $j-1$. Thus, the practical implementation of equation (38) is to add $-(\Delta t/\Delta x)\tilde{\lambda}_i \gamma_i \tilde{\mathbf{e}}_i$ to $\hat{\mathbf{w}}_{j-1}^m$, if $\tilde{\lambda}_i < 0$, to obtain $\hat{\mathbf{w}}_{j-1}^{m+1}$, or to add $-(\Delta t/\Delta x)\tilde{\lambda}_i \tilde{\gamma}_i \tilde{\mathbf{e}}_i$ to $\hat{\mathbf{w}}_j^m$, if $\tilde{\lambda}_i > 0$, to obtain $\hat{\mathbf{w}}_j^{m+1}$, for each computational cell (x_{j-1}, x_j) on the co-ordinate line $z = z_0$. The quantities $\tilde{\lambda}_i$, $\tilde{\mathbf{e}}_i$ represent approximations to the eigenvalues, and eigenvectors, respectively, of the Jacobian $\partial \hat{\mathbf{F}}/\partial \hat{\mathbf{w}}$ in the cell (x_{j-1}, x_j). These, together with the appropriate wavestrengths, $\tilde{\gamma}_i$, represent an extension of those contained in Section 4. The required expressions in (38) are

$$\tilde{\lambda}_{1,2} = \tilde{u} \pm \tilde{\psi}, \qquad \tilde{\mathbf{e}}_{1,2} = (1, \tilde{u} \pm \tilde{\psi}, \tilde{w})^{\mathrm{T}}, \tag{34a, b}$$

$$\tilde{\lambda}_3 = \tilde{u}, \qquad \tilde{\mathbf{e}}_3 = (0, 0, 1)^{\mathrm{T}}, \tag{34c}$$

$$\tilde{\gamma}_{1,2} = \frac{1}{2}\Delta\phi \pm \frac{1}{2}\frac{\tilde{\phi}}{\tilde{\psi}}\Delta u \mp \frac{g\tilde{\phi}}{2\tilde{\psi}(\tilde{u} \pm \tilde{\psi})}(\Delta h - \tilde{s}_x \Delta x), \tag{35a, b}$$

$$\tilde{\gamma}_3 = \tilde{\phi}\,\Delta w \tag{35c}$$

and

$$\tilde{s}_x = \frac{g^{4/3} n^2 \sqrt{(\tilde{u}^2 + \tilde{w}^2)}}{\tilde{\phi}^{4/3}} \quad \text{or} \quad \frac{g\sqrt{(\tilde{u}^2 + \tilde{w}^2)}}{\tilde{\phi} C^2}, \tag{36a, b}$$

where the approximations to u, w, ϕ and $\sqrt{\phi}$ in (x_{j-1}, x_j) are given by

$$\tilde{Z} = \frac{\sqrt{(\phi_{j-1})} Z_{j-1} + \sqrt{(\phi_j)} Z_j}{\sqrt{(\phi_{j-1})} + \sqrt{(\phi_j)}}, \quad Z = u \quad \text{or} \quad w, \tag{37a, b}$$

$$\tilde{\phi} = \sqrt{(\phi_{j-1}\phi_j)} \tag{38}$$

and

$$\tilde{\psi} = \sqrt{[\tfrac{1}{2}(\phi_{j-1} + \phi_j)]}, \tag{39}$$

respectively. The differences are defined by

$$\Delta Z = Z(x_j, z_0) - Z(x_{j-1}, z_0), \qquad Z = \phi, u, w, h. \tag{40}$$

The corresponding scheme for equation (32b), together with the resulting values of $\tilde{\lambda}_i$, $\tilde{\gamma}_i$ and $\tilde{\mathbf{e}}_i$, can easily be deduced by symmetry. Second-order extensions are achieved as for the one-dimensional scheme in Section 4.

6. TEST PROBLEMS

We consider three test problems to assess the schemes presented in Sections 4 and 5.

Problem 1

Consider a wide, frictionless channel whose bottom surface is flat, and a barrier placed across its width. The water on one side of the barrier is at a different height to that on the other. At time $t=0$, the barrier is removed and the resulting flow consists of a bore travelling downstream and a depression wave travelling upstream.[1] To treat this one-dimensional problem numerically consider a fixed region $0 \leqslant x \leqslant 1$ with a barrier at $x=0{\cdot}5$. The upstream water height is ϕ_1 and the downstream water height is ϕ_0, as represented in Figure 1. The governing equations are given by equation (1) with $\mathbf{b}=\mathbf{0}$. The assumption of zero friction is made so that the numerical solution can

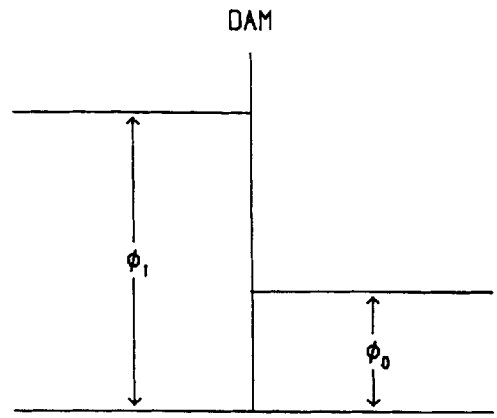

Figure 1. A schematic representation of the dam in Problem 1

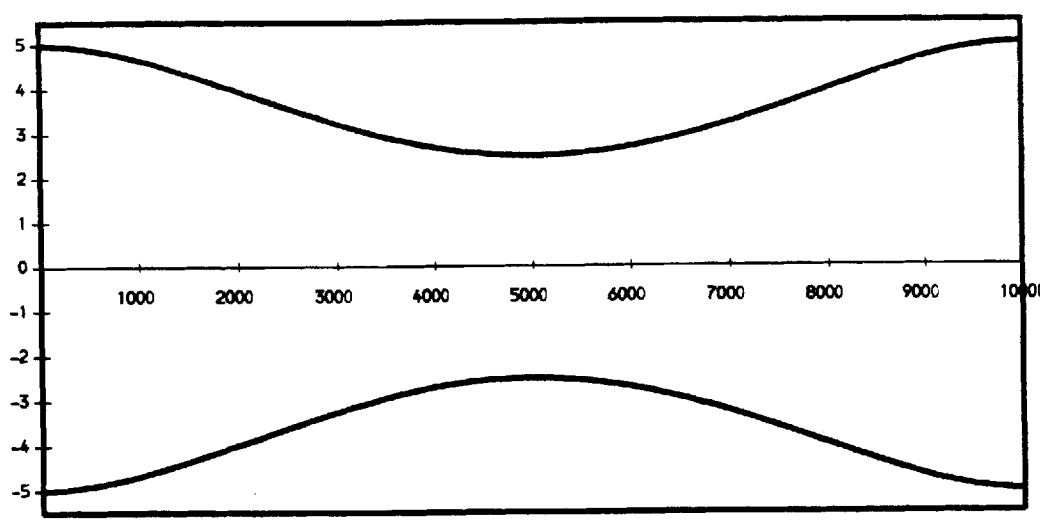

Figure 2. Channel breadth in Problem 2

be compared with the exact solution[1] and the ratio ϕ_1/ϕ_0 determines whether the flow downstream of the barrier is subcritical or supercritical. (A region of flow is said to be supercritical if both eigenvalues λ_1, λ_2 given by equations (15a) and (15b) are of the same sign, i.e. when $|u| > \sqrt{\phi}$; otherwise, the flow is said to be subcritical.) For large values of the ratio ϕ_1/ϕ_0 the flow downstream of the barrier becomes supercritical and the bore can be difficult to capture. (The speed of the bore is the speed at which the discontinuity in the solution travels.) In particular, the speed of the bore is not always correctly determined.[4]

Problem 2

Consider the flow in a channel with a smooth constriction and a sloping bottom surface, which shelves. This geometry induces a flow which becomes supercritical and the governing equations are given by equation (1). The channel is 10 000 m long, and the breadth, B, varies from 10 m to 5 m to 10 m (see Figure 2). The bed slope is taken to be a constant value, except between 4500 and 5500 m, where twice this value is taken (see Figure 3). Only one boundary condition needs to be applied to each end of the channel. At the left-hand end the mass flow, Q, is specified, and at the right-hand end the depth, d, is specified by extrapolation from the interior.

Problem 3

This is a two-dimensional dam-break problem with a non-symmetrical breach. The computational domain is defined by a channel 200 m long and 200 m wide and the governing equations are given by equation (26). The non-symmetrical breach is 75 m and the dam is 10 m thick, as shown in Figure 4. Initially, the water is at different heights ϕ_0, ϕ_1 on either side of the breach. For the purposes of comparison with other schemes, we consider a horizontal, frictionless channel.

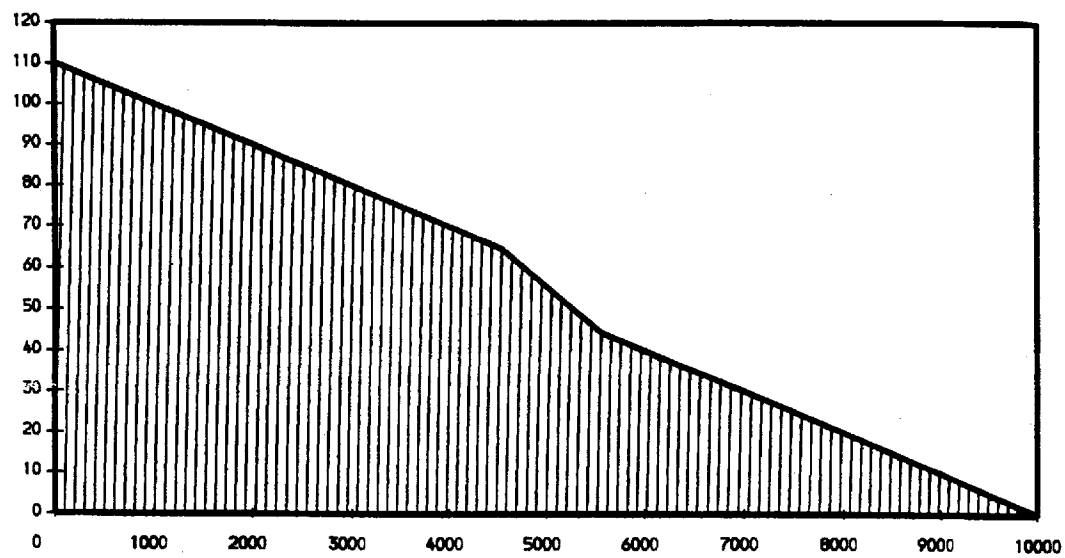

Figure 3. Channel cross-section in Problem 2

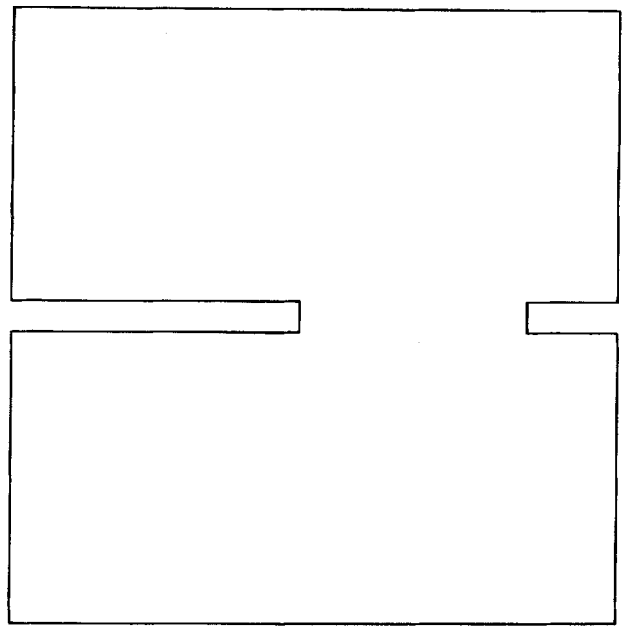

Figure 4. The computational domain for Problem 3

7. NUMERICAL RESULTS

Numerical results are given for the three problems of Section 6 using the finite difference schemes of Sections 4 and 5.

Problem 1

Various ratios of ϕ_1/ϕ_0 are taken in order to include both subcritical and supercritical flows. In each case the 'Superbee' limiter[11] has been used so that the resulting scheme is second-order-accurate, but no spurious oscillations are produced. The results, together with the exact solution, are given in Figures 5–11. Figures 5–9 represent the cases $\phi_1/\phi_0 = 2, 5, 10, 20$ and 100, respectively, where $\phi_1 = 1$ and 50 mesh points have been used. The approximate solution gives a good representation of the exact solution in each case. In the case $\phi_1/\phi_0 = 100$, where the downstream flow is supercritical, there is a lack of resolution and the solution is significantly improved using 100 mesh points as in Figure 10. For supercritical cases, i.e. values of $\phi_1/\phi_0 > 7{\cdot}2$, 100 mesh points are generally needed to obtain a good approximation to the exact solution. This can be seen for the case $\phi_1/\phi_0 = 250$ in Figure 11. All figures are at $t = 0{\cdot}25$. The numerical results compare well with the results given by other authors.[4]

Problem 2

Figures 12–14 show the results for Problem 2 for a slope of 0·01, and the mass flow, Q, the depth, d, and the Froude number, $Fr = u/\sqrt{(gd)}$, are all displayed. Figures 15–17 show the corresponding results for a slope of 0·02. Both sets of results are for 100 mesh points, a mass flow

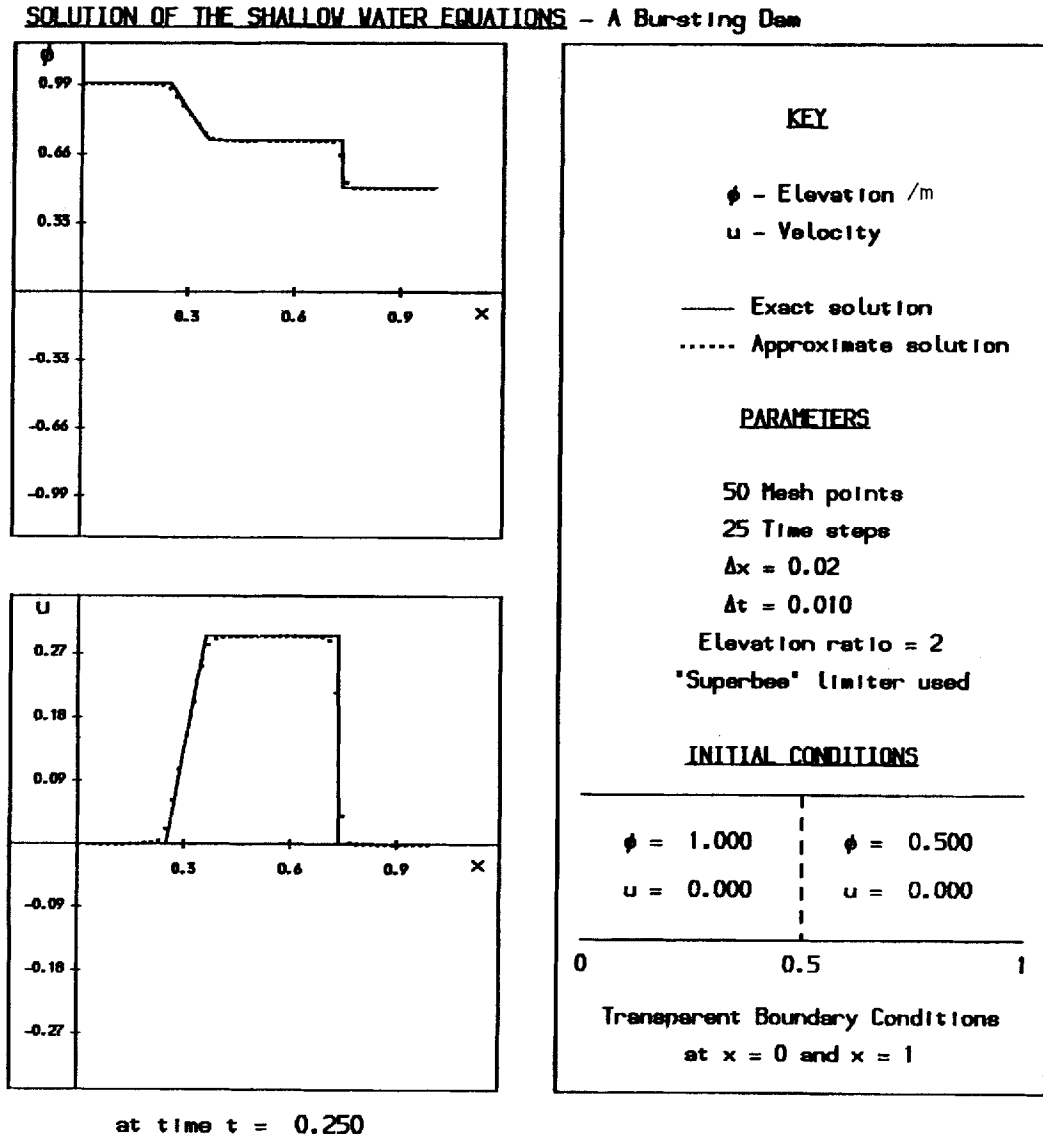

Figure 5. Solution of Problem 1 with $\phi_1/\phi_0=2$ and 50 mesh points

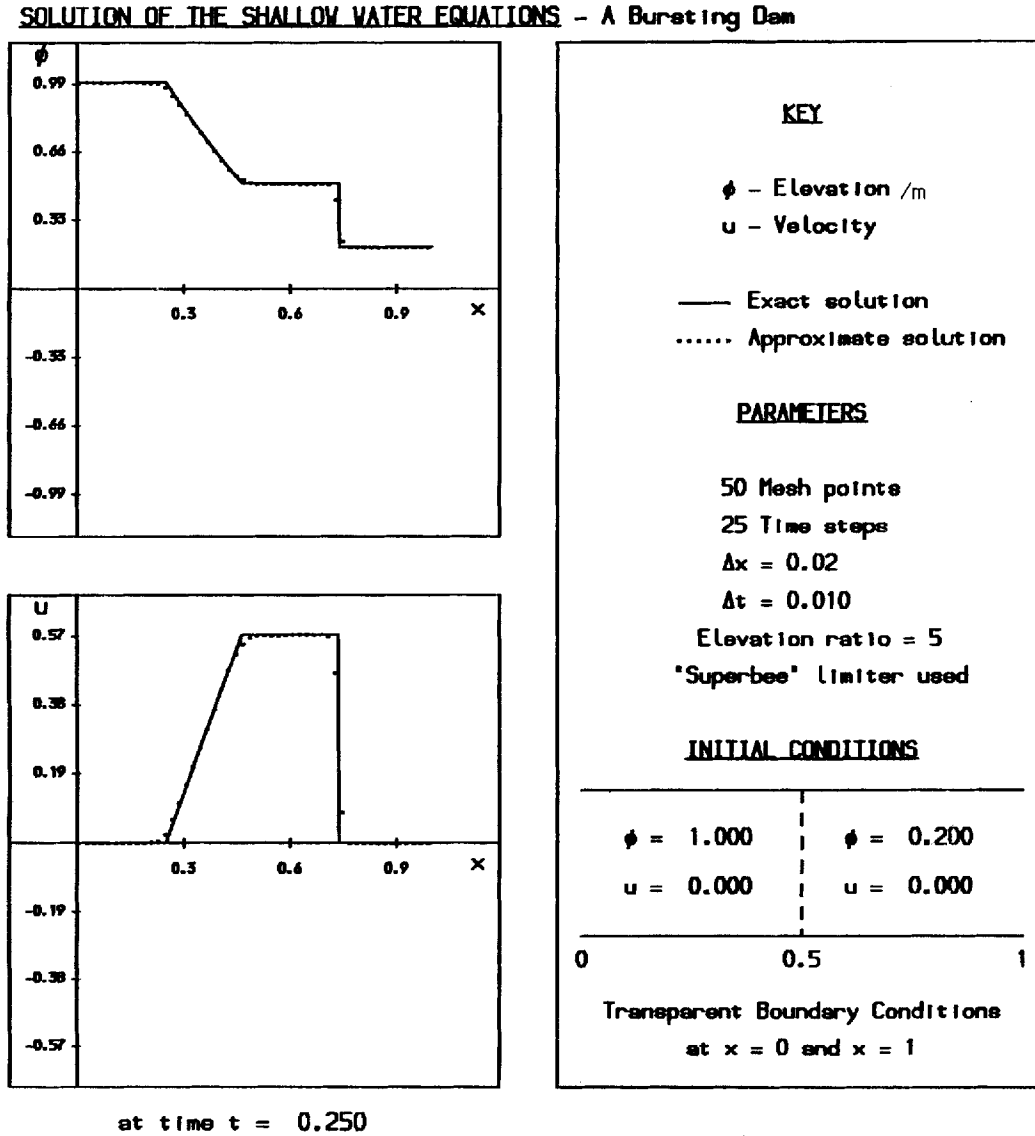

Figure 6. Solution of Problem 1 with $\phi_1/\phi_0 = 5$ and 50 mesh points

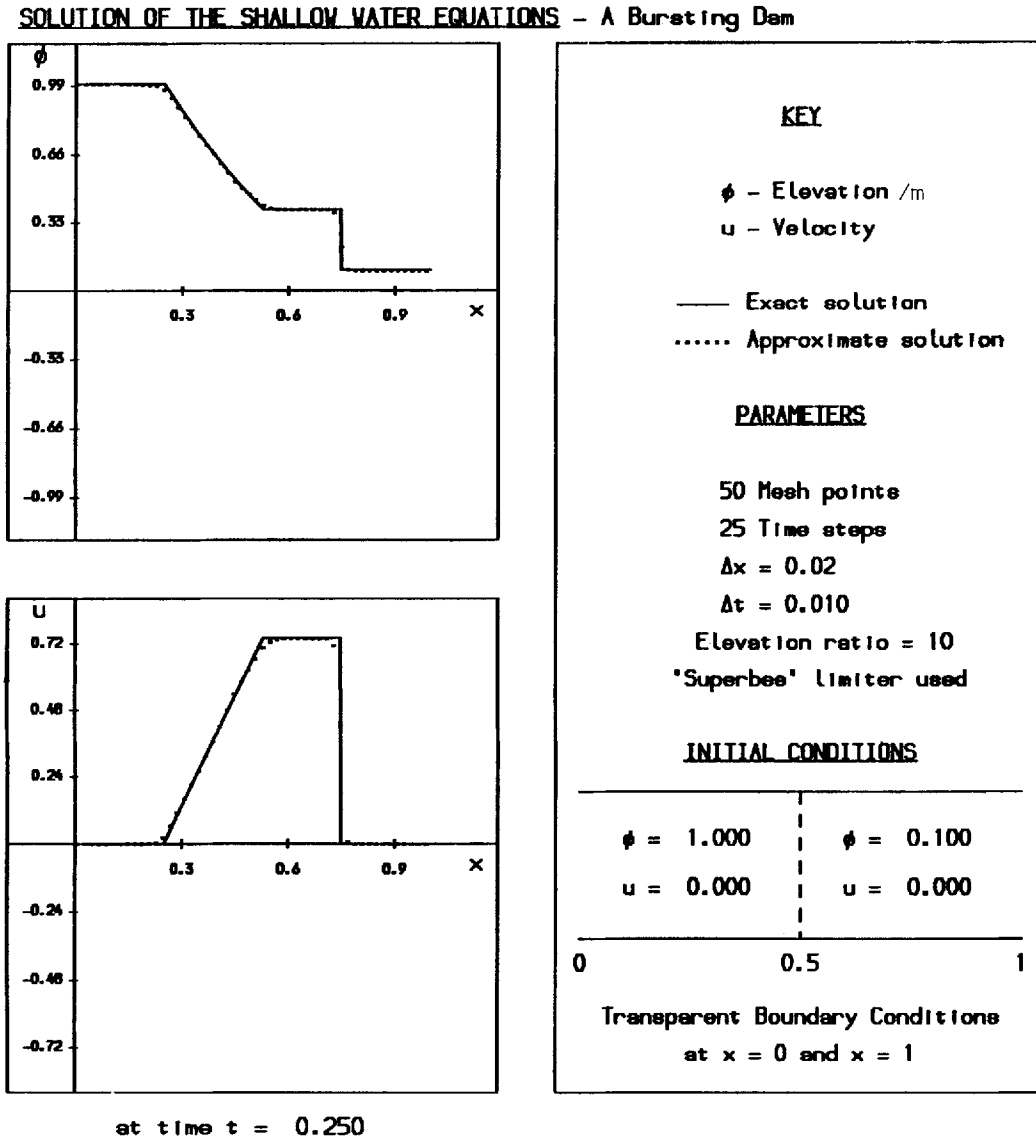

Figure 7. Solution of Problem 1 with $\phi_1/\phi_0 = 10$ and 50 mesh points

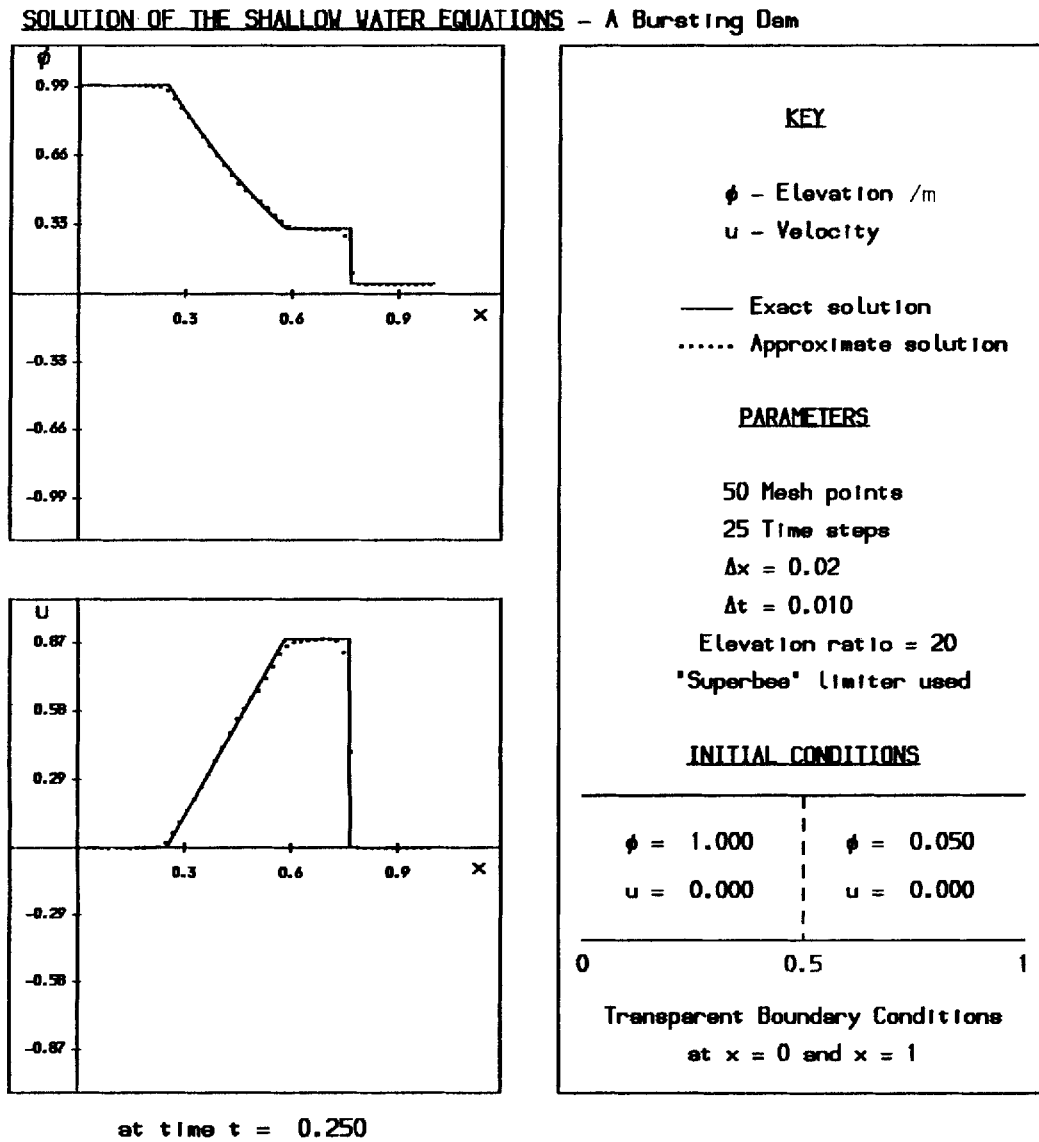

Figure 8. Solution of Problem 1 with $\phi_1/\phi_0 = 20$ and 50 mesh points

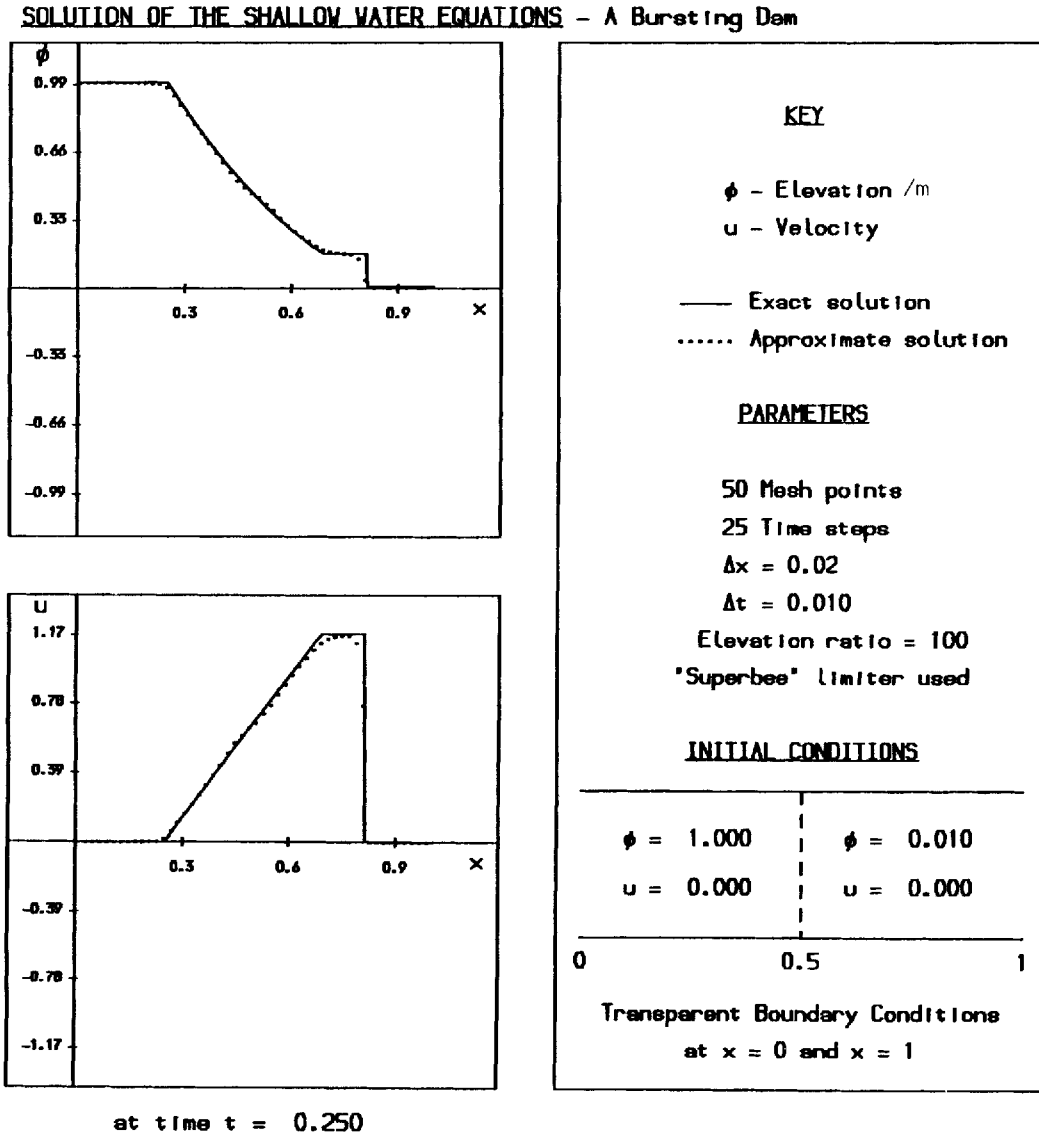

Figure 9. Solution of Problem 1 with $\phi_1/\phi_0 = 100$ and 50 mesh points

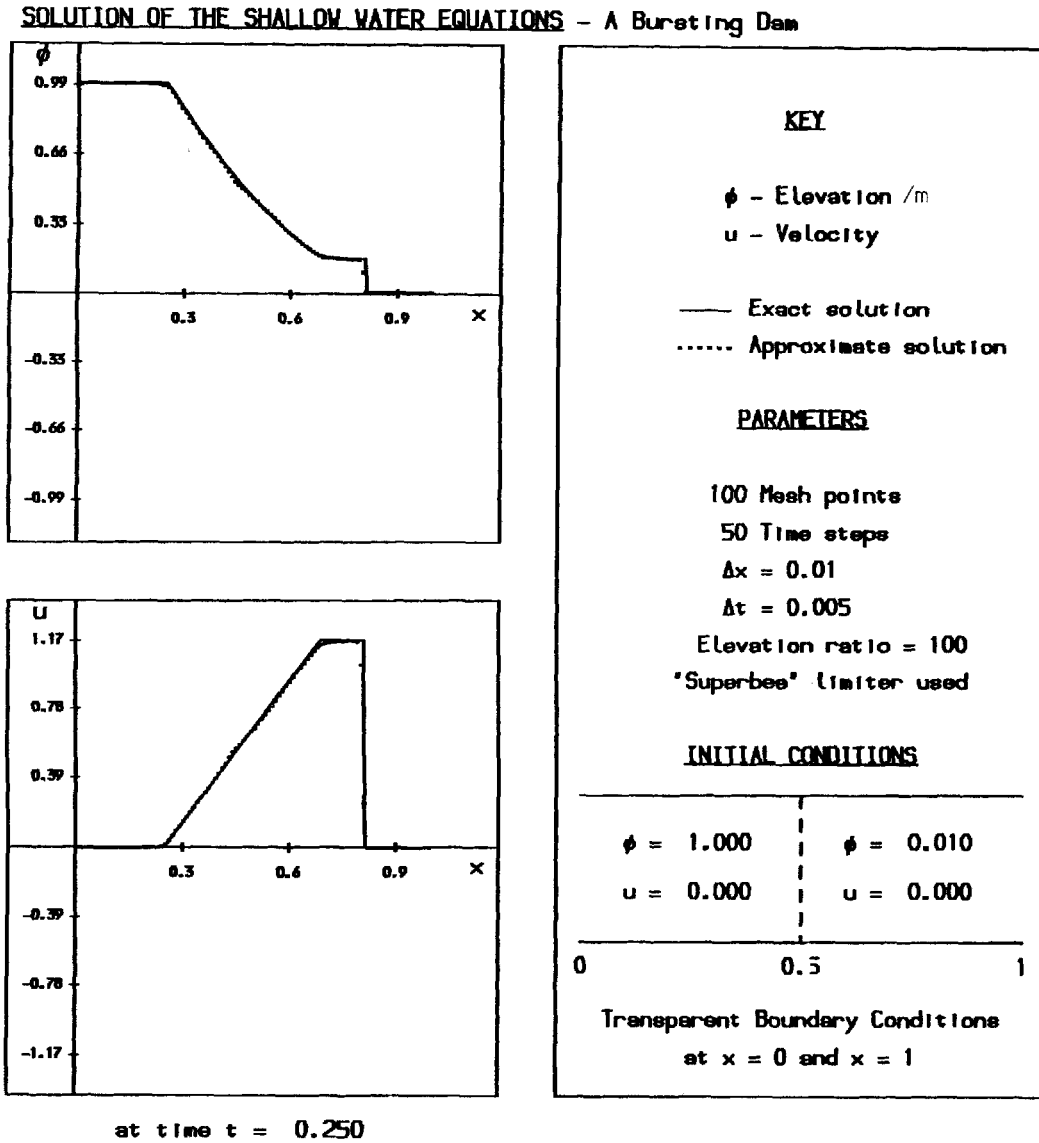

Figure 10. Solution of Problem 1 with $\phi_1/\phi_0 = 100$ and 100 mesh points

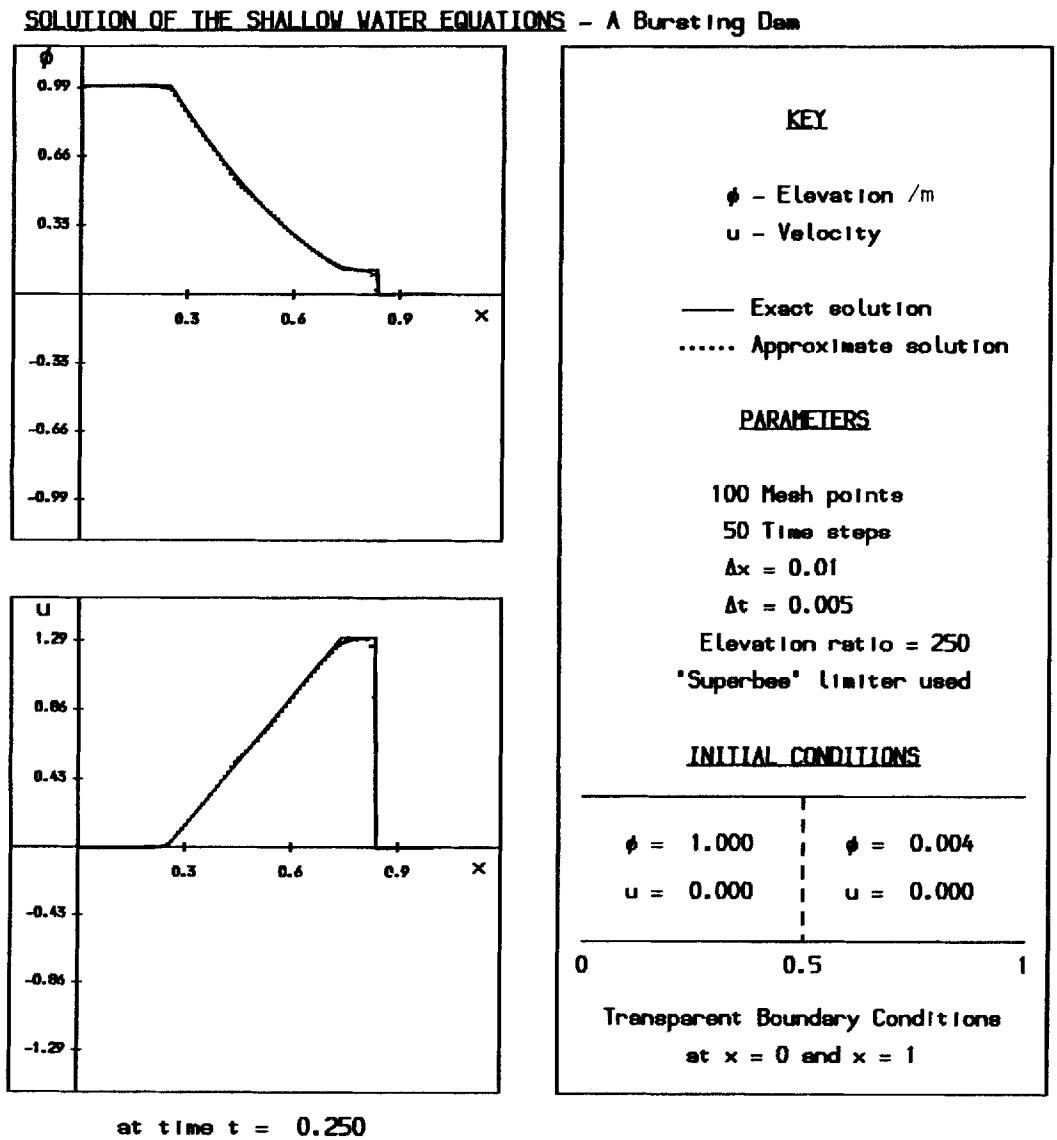

Figure 11. Solution of Problem 1 with $\phi_1/\phi_0 = 250$ and 100 mesh points

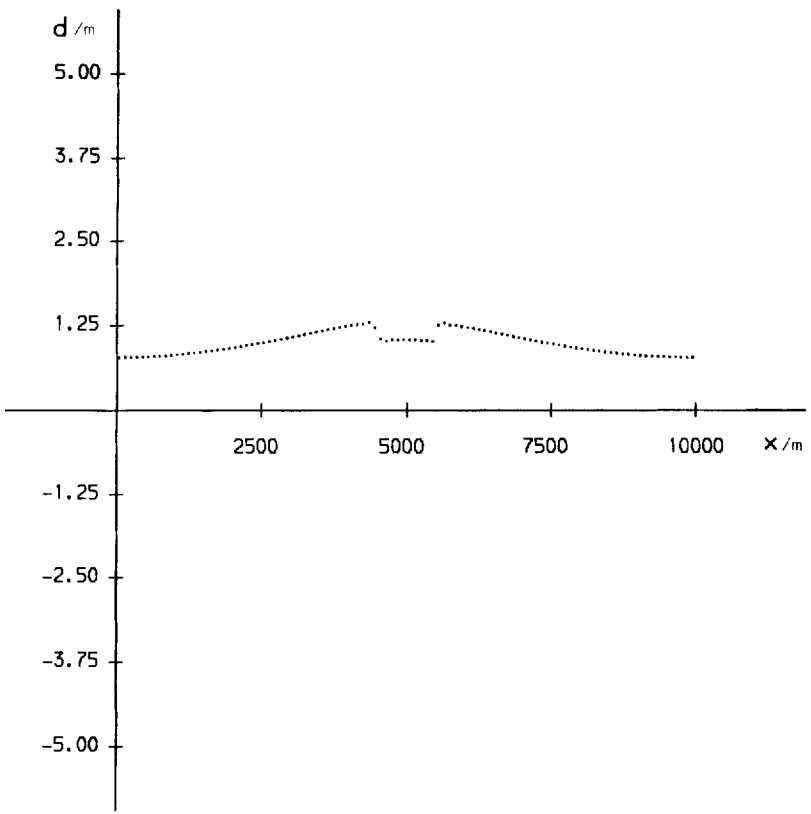

Figure 12. A plot of depth, d(m), for a bed-slope of 0·01 for Problem 2 using the method of Section 4

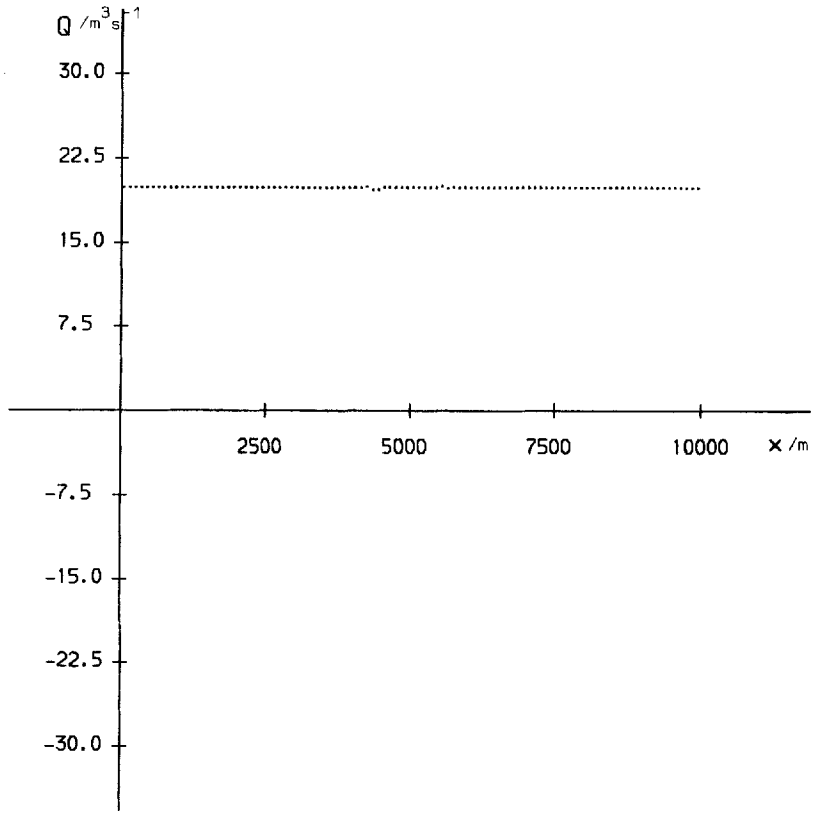

Figure 13. A plot of mass flows, $Q(\mathrm{m^3\,s^{-1}})$, for a bed-slope of 0·01 for Problem 2 using the method of Section 4

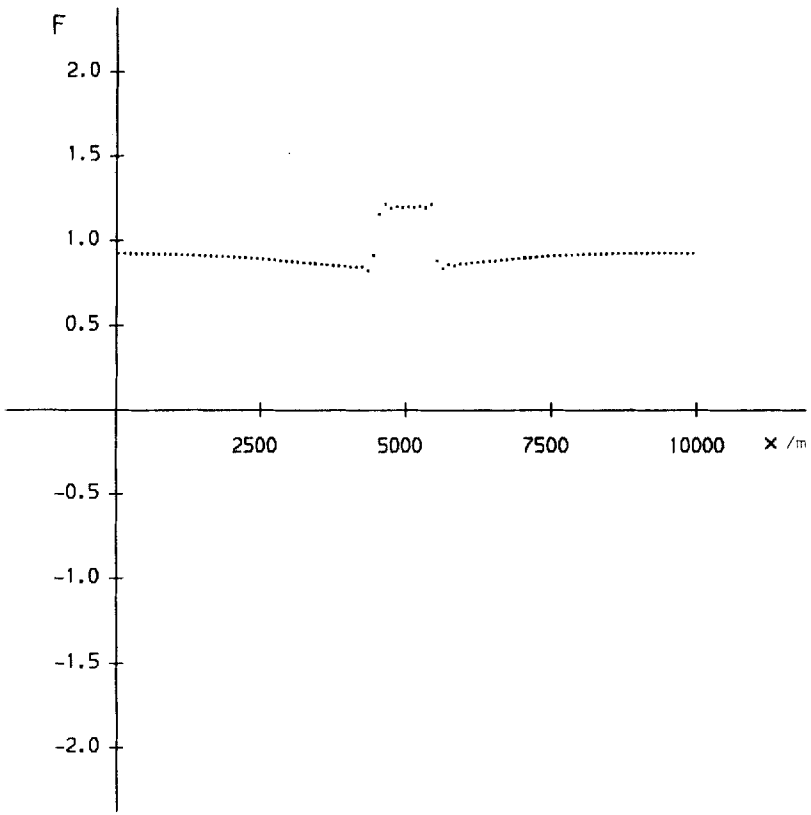

Figure 14. A plot of Froude number, Fr, for a bed-slope of 0·01 for Problem 2 using the method of Section 4

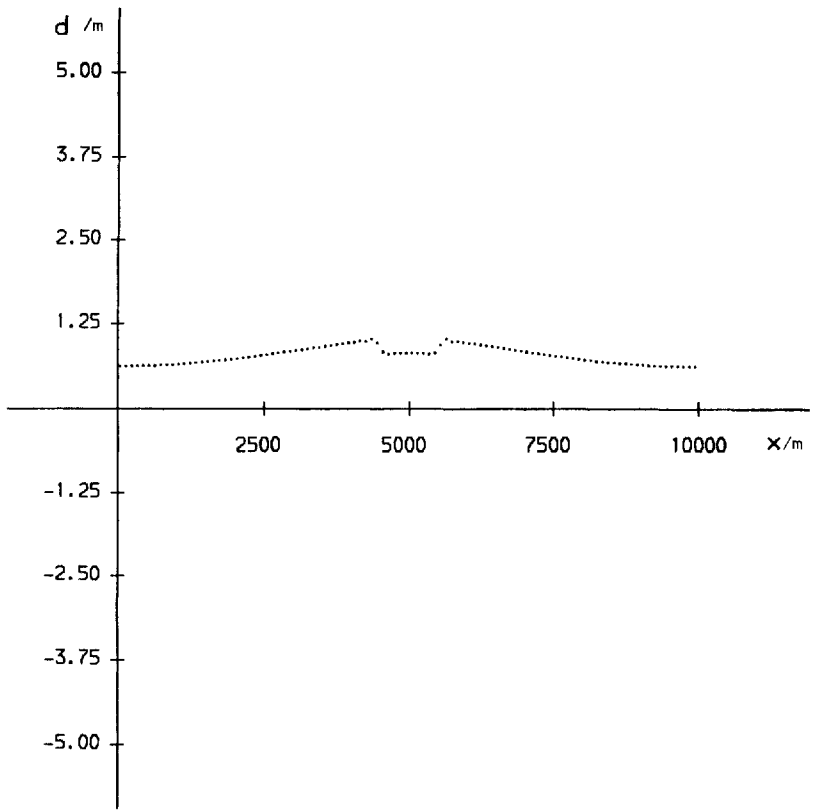

Figure 15. A plot of depth, d(m) for a bed-slope of 0·02 for Problem 2 using the method of Section 4

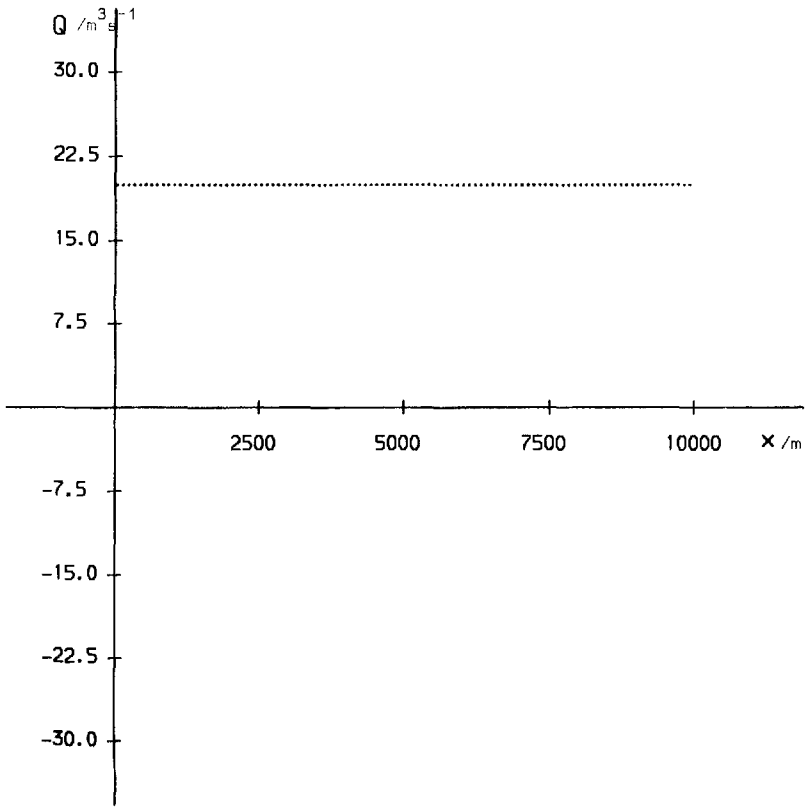

Figure 16. A plot of mass flow, Q ($m^3 s^{-1}$), for a bed-slope of 0·02 for Problem 2 using the method of Section 4

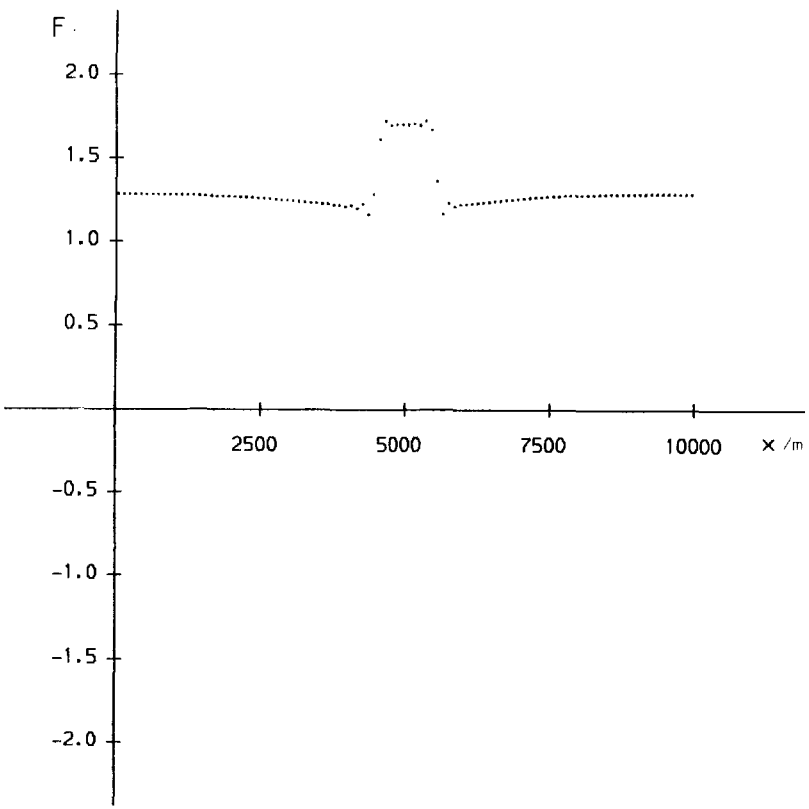

Figure 17. A plot of Froude number, Fr, for a bed-slope of 0·02 for Problem 2 using the method of Section 4

of 20 m^3/s and after a time of 3000 s. We see that the flow has reached a steady state, with a good prediction of the flow, even though it is supercritical in some, or all, of the channel. These results compare well with those of other authors, and Figures 18–23 show the corresponding results using the algorithm in Reference 13.

Problem 3

Two sets of initial conditions are chosen here: (a) $\phi_1/g=10$, $\phi_0/g=5$ and (b) $\phi_1/g=10$, $\phi_0/g=0{\cdot}05$, representing tailwater/reservoir height ratios of 0·5 and 0·005, respectively, and a grid

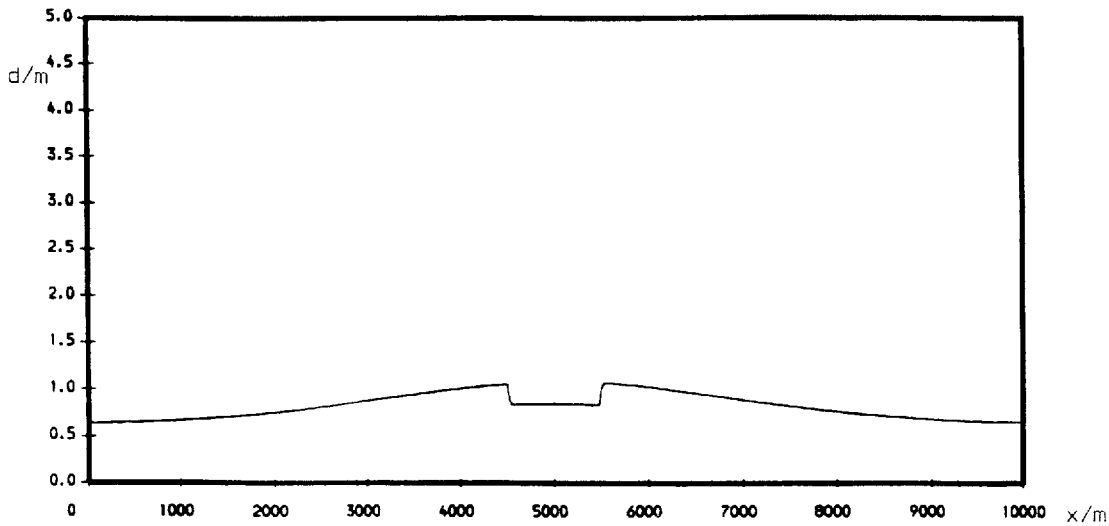

Figure 18. A plot of depth, d(m) for a bed-slope of 0·01 for Problem 2 using the method in Reference 13

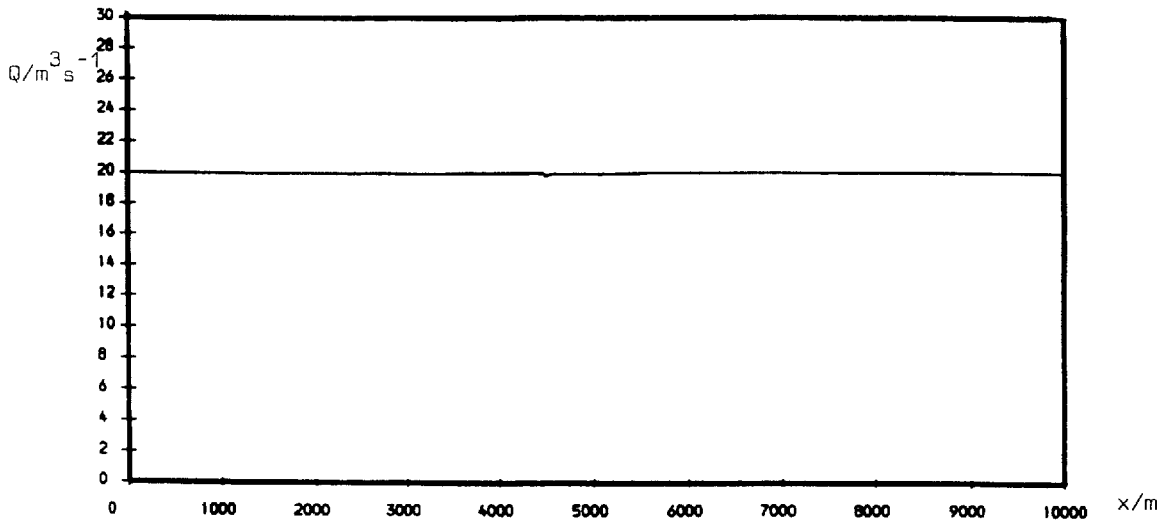

Figure 19. A plot of mass flow, $Q(m^3 s^{-1})$, for a bed-slope of 0·01 for Problem 2 using the method in Reference 13.

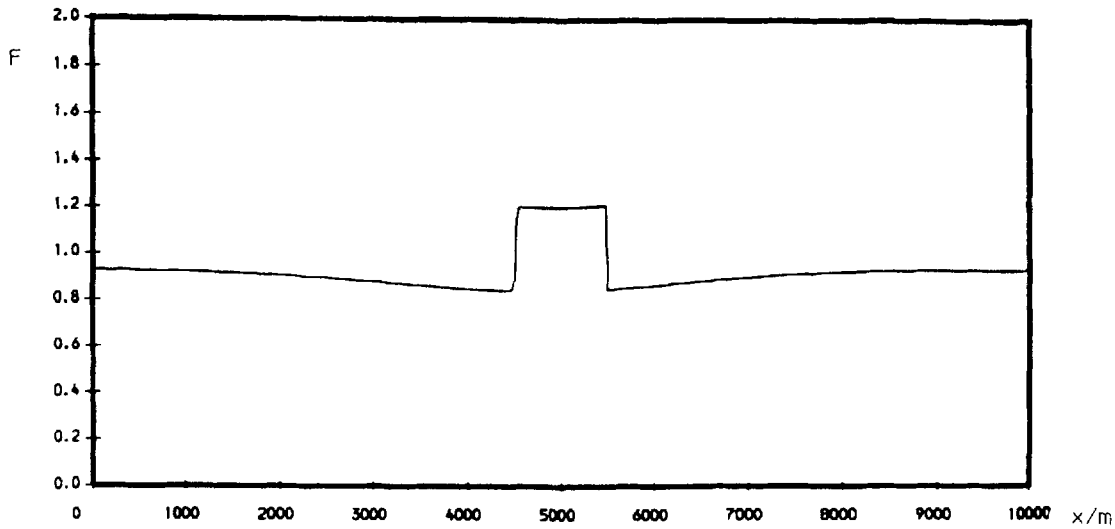

Figure 20. A plot of Froude number, Fr, for a bed-slope of 0·01 for Problem 2 using the method in Reference 13

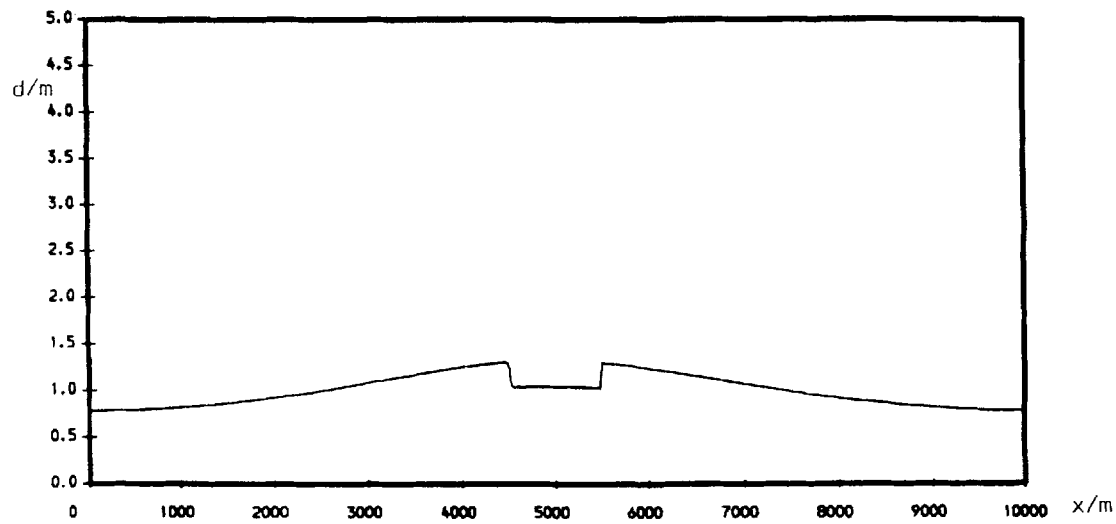

Figure 21. A plot of depth, d(m), for a bed-slope of 0·02 for Problem 2 using the method in Reference 13

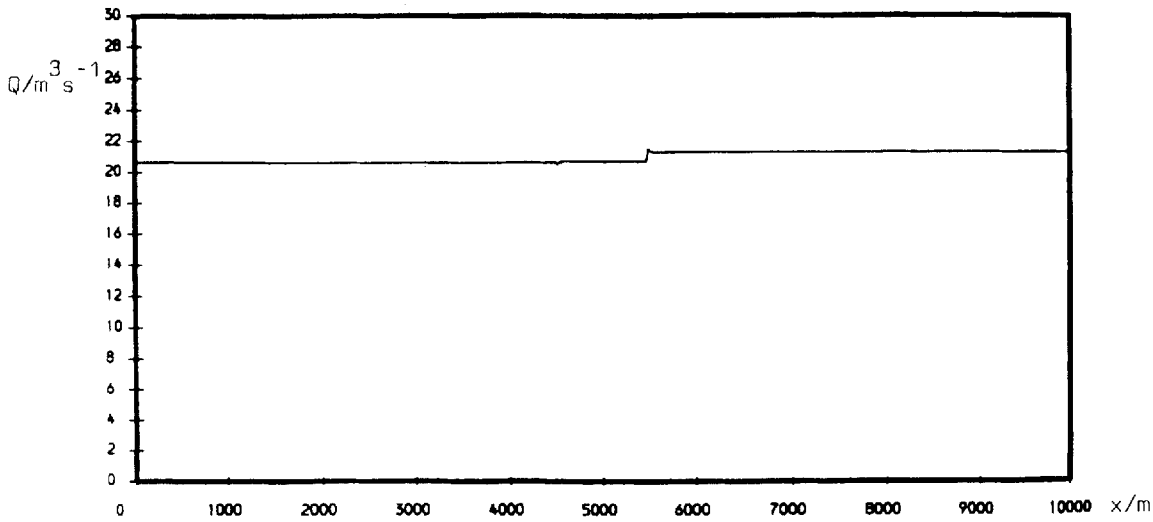

Figure 22. A plot of mass flow, $Q(\mathrm{m^3\,s^{-1}})$, for a bed-slope of 0·02 for Problem 2 using the method in Reference 13

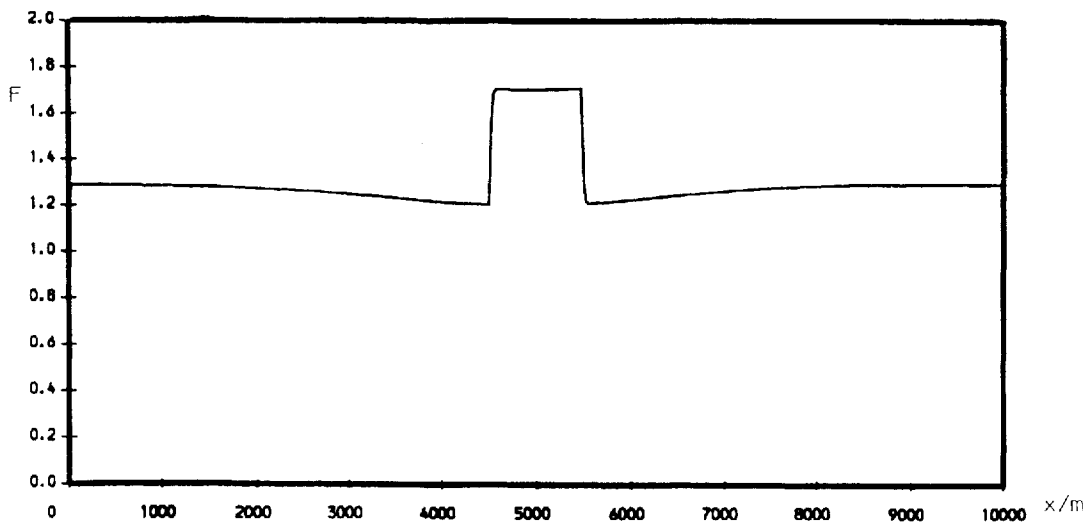

Figure 23. A plot of Froude number, Fr, for a bed-slope of 0·02 for Problem 2 using the method in Reference 13

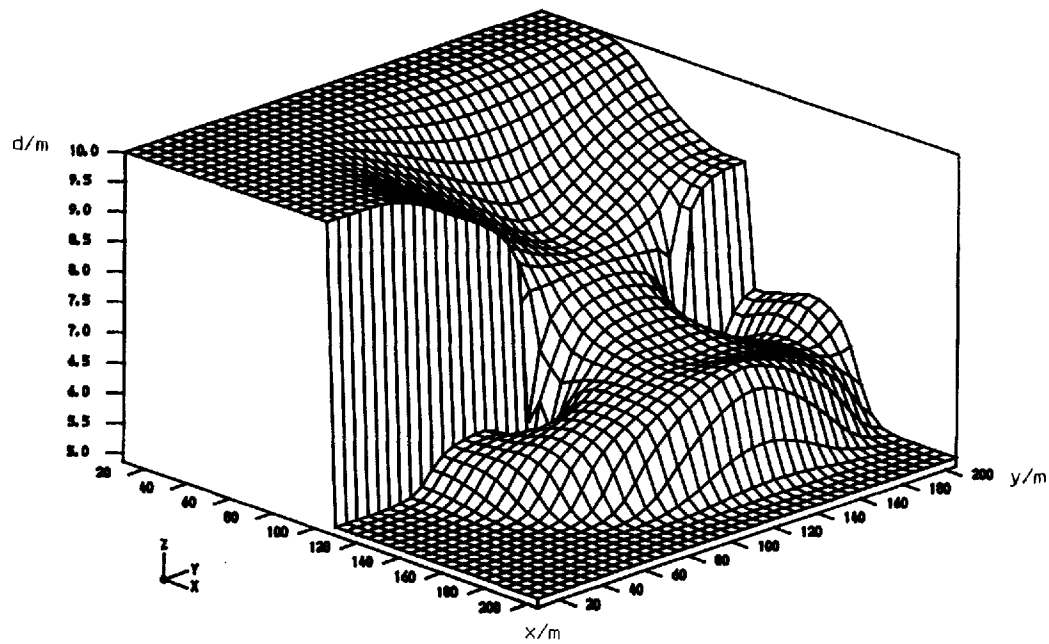

Figure 24. Contours of surface elevation for a tailwater/reservoir height ratio of 0·5 at time 7·1 s for Problem 3

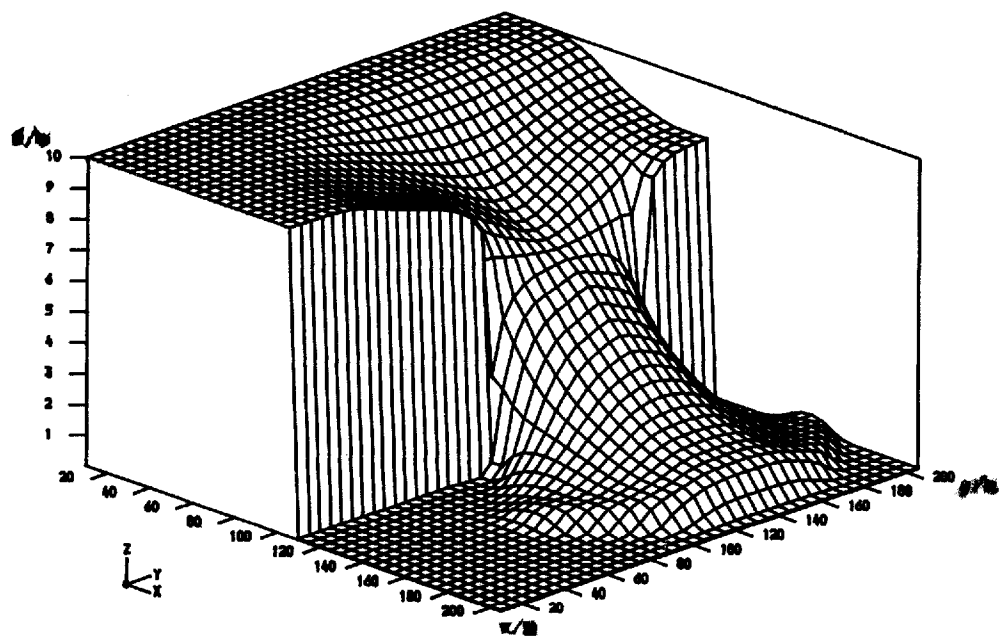

Figure 25. Contours of surface elevation for a tailwater/reservoir height ratio of 0·005 at time 7·1 s for Problem 3

of 41×41 points results in a mesh size of 5×5 m. The results displaying surface elevation contours for these two cases are shown in Figures 24 and 25, respectively, at time $t = 7{\cdot}1$ s. (N.B. The figures display contours where the dam is still intact since it is not possible to mask these areas.) In both cases we see that the bore has developed well. Only in case (a) is there significant reflection from the wall. This compares favourably with the results found by Fennema and Chaudry for the case where the bore is smeared over a number of cells. It is noted by these authors that many numerical schemes have difficulty in computing accurate solutions, if any, for small ratios of tailwater/reservoir height.

The explicit finite difference scheme of Sections 4 and 5 is computationally efficient and the c.p.u. time taken to compute the results for Problem 2, for example, was as follows. Using an Amdahl V7 with 100 mesh points takes 0·0096 c.p.u. seconds to compute one time step and a total of 2·88 c.p.u. seconds to reach a real time of 3000 s using 300 time steps, each of 10 s.

8. CONCLUSIONS

A conservative finite difference scheme is presented for the solution of the one- and two-dimensional shallow-water equations in open channels based on flux difference splitting. By considering linearized Riemann problems, and solving these approximately using upwind differencing, enables the geometry-induced supercritical flow in an open channel, and the flow resulting in a dam break, to be predicted satisfactorily. The resulting scheme is computationally efficient and can be used with confidence to predict accurate solutions to open-channel flow problems.

APPENDIX

Here we derive the averages given in Section 4.2. Multiplying out equation (9a) gives

$$\Delta(Au) = \Delta(Au) \tag{41}$$

and

$$-\tilde{u}^2 \Delta A + 2\tilde{u}\,\Delta(Au) = \Delta(Au^2). \tag{42}$$

Equation (41) is an identity, and equation (42) is a quadratic equation for $\tilde{u}$ with roots

$$\tilde{u} = \frac{\Delta(Au) \pm \sqrt{\{[\Delta(Au)]^2 - (\Delta A)[\Delta(Au^2)]\}}}{\Delta A}$$

$$= \frac{\Delta(Au) \pm \sqrt{(A_R A_L)}\Delta u}{\Delta A}, \tag{43}$$

after simplifying the discriminant. With the plus sign no simple formula results. However, with the minus sign, the numerator in equation (43) can be simplified as

$$\Delta(Au) - \sqrt{(A_R A_L)}\Delta u = (\sqrt{A_R} - \sqrt{A_L})(\sqrt{(A_R)}u_R + \sqrt{(A_L)}u_L), \tag{44}$$

and since

$$\Delta A = A_R - A_L = (\sqrt{A_R} + \sqrt{A_L})(\sqrt{A_R} - \sqrt{A_L}), \tag{45}$$

equation (43) with the minus sign, together with equations (44) and (45), imply that

$$\tilde{u} = \frac{\sqrt{(A_R)}u_R + \sqrt{(A_L)}u_L}{\sqrt{A_R} + \sqrt{A_L}}, \tag{46}$$

as in equation (11).

Finally, from equation (9b)

$$\tilde{A}\,\Delta A = \Delta(A^2/2), \tag{47}$$

and, hence,

$$\tilde{A} = \frac{\Delta(A^2/2)}{\Delta A} = \frac{1}{2}\frac{(A_R^2 - A_L^2)}{A_R - A_L} = \tfrac{1}{2}(A_R + A_L), \tag{48}$$

as in equation (12).

REFERENCES

1. J. J. Stoker, *Water Waves*, Interscience Publishers, Wiley, New York, 1957.
2. M. B. Abbott, *Computational Hydraulics: Elements of the Theory of Free-Surface Flows*, Pitman, London, 1979.
3. J. Cunge, F. M. Holley and A. Verwey, *Practical Aspects of Computational River Hydraulics*, Pitman, London, 1980.
4. R. J. Fennema and M. H. Chaudry, 'Simulation of one-dimensional dam-break flows', *J. Hydraul. Res.*, **25**, 41–51 (1987).
5. A. Preissman, 'Propagation des intumescences dans les canaux et rivieres', Paper presented at the First Congress of the French Association for Computation, Grenoble, France, 1961.
6. J. Goussebaile and F. Lepeintre, 'A method to solve the one-dimensional shallow water equations using characteristics and flux splitting', in R. A. Falconer, P. Goodwin and R. G. S. Matthew (eds), *Hydraulic and Environmental Modelling of Coastal, Estuarine and River Waters, Proc. of the Int. Conf.*, Bradford, Gower Technical, 1989.
7. P. Glaister, 'An approximate linearised Riemann solver for the one-dimensional Euler equations with real gases', *J. Comput. Phys.*, **74**, 382–408 (1988).
8. J. P. Vila, 'Simplified Godunov schemes for 2×2 systems of conservation laws', *SIAM J. Numer. Anal.*, **23**, 1173 (1986).
9. J. P. Vila, 'Schemas numeriques en hydraulique des ecoulements avec discontinuities', in J. A. Cunge and P. Ackers (eds), *Proc. XII Congress IAHR*, Lausanne, 1987.
10. S. K. Godunov, 'A difference method for the numerical computation of continuous solutions of hydrodynamic equations', *Mat. Sbornik*, **47**, 271–306 (1959) (Translated as JPRS 7225 by U.S. Dept. of Commerce, 1960).
11. P. K. Sweby, 'High resolution schemes using flux limiters for hyperbolic conservation laws', *SIAM J. Numer. Anal.*, **21**, 995 (1984).
12. P. K. Sweby, 'A modification of Roe's scheme for entropy satisfying solutions of scalar non-linear conservation laws', *Numerical Analysis Report*, University of Reading, 1982.
13. A. Priestley, 'A quasi-Riemann method for supercritical, open channel flow', *Numerical Analysis Report*, University of Reading, (submitted to *J. Comput. Phys.*), 1991.
14. R. J. Fennema and M. H. Chaudry, 'Implicit methods for two dimensional unsteady free-surface flows', *J. Hydraul. Res.*, **27**, 321–332 (1989).